Journal of the Optical Society of America B
OPTICAL PHYSICS

Generation of millijoule few-cycle pulses at 5 μm by indirect spectral shaping of the idler in an optical parametric chirped pulse amplifier

MARTIN BOCK, LORENZ VON GRAFENSTEIN, UWE GRIEBNER,* AND THOMAS ELSAESSER

Max Born Institute for Nonlinear Optics and Short Pulse Spectroscopy, Max-Born-Str. 2a, D-12489 Berlin, Germany
**Corresponding author: griebner@mbi-berlin.de*

Received 12 July 2018; revised 12 September 2018; accepted 16 September 2018; posted 17 September 2018 (Doc. ID 338698); published 11 October 2018

Spectral pulse shaping in a high-intensity midwave-infrared (MWIR) optical parametric chirped pulse amplifier (OPCPA) operating at 1 kHz repetition rate is reported. We successfully apply a MWIR spatial light modulator (SLM) for the generation of ultrashort idler pulses at 5 μm wavelength. Only bulk optics and active phase control of the 3.5 μm signal pulses via the SLM are employed for generating compressed idler pulses with a duration of 80 fs. The 80-fs pulse duration corresponds to less than five optical cycles at the central wavelength of 5.0 μm. The pulse energy amounts to 1.0 mJ, which translates into a peak power of 10 GW. The generated pulse parameters represent record values for high-intensity MWIR OPCPAs.

https://doi.org/10.1364/JOSAB.35.000C18

1. INTRODUCTION

In recent years, an increasing number of parametric sources of few-cycle mid-infrared (MIR) pulses have been implemented. This development has opened new possibilities in research on strong-field laser-matter interactions [1]. These mid-infrared sources are ideal tools for 2D infrared spectroscopy, time-resolved imaging of molecular structures, the generation of high harmonics, and the advancement of novel x-ray sources [2–5]. The generation of intense few-cycle midwave (MWIR, $\lambda = 3$–8 μm) and longwave infrared (LWIR, $\lambda = 8$–15 μm) pulses is one of the current challenges to ultrafast laser technology. Presently, the majority of high-peak-power few-cycle sources rely on optical parametric amplifiers (OPAs) or optical chirped pulse parametric amplifiers (OPCPAs) pumped by 1-μm lasers. However, these parametric amplifiers face significant challenges with an increase of the output wavelength beyond 4 μm due to a lack of suitable nonlinear crystals [6–10]. To generate high-intensity pulses in the MWIR and LWIR spectral region via OPA or OPCPA, non-oxide crystals such as zinc germanium phosphide (ZGP) or cadmium silicon phosphide (CSP) have to be used [11]. These crystals display large second-order nonlinearities but demand adequate high-performance pump lasers, which emit at wavelengths above 2 μm [4,12]. Another key feature is the spectral phase control to achieve few-cycle pulse durations. For this purpose, active optical elements such as liquid crystal (LC) arrays and acousto-optic programmable dispersive filters (AOPDF) in pulse shaper arrangements have to be implemented. These devices have enabled the required phase control in numerous experiments in the visible and near-IR [13–17]. In contrast, only very few parametric amplifier systems are reported, which generate intense few-cycle pulses at wavelengths $\lambda > 4$ μm.

Pulses around 5 μm have been generated at a 1-kHz repetition rate with durations of 13 fs [18] and 99 fs [19] and energies of 33 μJ [18] and 40 μJ [19], respectively. In the described systems, an AOPDF is used to shape the 2-μm pump pulses. Without active spectral phase control, 160-fs, 860-μJ [20] and 180-fs, 200-μJ [21] pulses were generated at central wavelengths of 5 μm and 7 μm, respectively. In comparison to the other referenced systems, the 7-μm OPCPA setup was operated at a rather low repetition rate of 0.1 kHz. Similarly, the 10-Hz OPCPA system in [22] indicates the importance to spectral phase control of the MWIR pulses for approaching the Fourier-transform limit (FTL). Pulses with a duration of 450 fs and 50 μJ energy were generated corresponding to ∼10 times the FTL for the generated 5-μm pulses.

Here we present spectral pulse shaping using a LC-array-based spatial light modulator (SLM) in the MWIR. This SLM allows a more straightforward phase manipulation for the broadband signal pulses at 3.5 μm compared to the idler pulses. Due to the chirp transfer during parametric amplification, we thus indirectly manage the dispersion of the 5-μm idler pulses and recompress them to a sub-100-fs few-cycle duration.

2. EXPERIMENTAL SETUP AND PERFORMANCE OF THE 2-μm PUMP SOURCE

The conceptual scheme of the MWIR OPCPA system and the design of the pulse shaper are displayed in Fig. 1. A three-color front end based on a femtosecond Er:fiber master oscillator operating at 40 MHz serves as seed for the 2-μm pump channel and the difference frequency generation (DFG) of seed pulses at 3.6 μm for the OPCPA. In the pump channel, the supercontinuum seed pulses are amplified by a single Tm:fiber amplifier and stretched by a chirped volume Bragg grating, resulting in pulses with energy of 0.5 nJ, ~1 ns duration, and 13 nm spectral width (full width at half-maximum, FWHM). The pulses are fed into the Ho:YLF amplifier chain of the chirped pulse amplifier (CPA) system operating at a 1-kHz repetition rate. All main amplifiers are running at room temperature and are pumped by continuous-wave Tm:fiber lasers at 1940 nm. At first, the pulses are amplified to 10 mJ by a regenerative amplifier. The pulse energy is further linearly scaled to >50 mJ by two single-pass booster amplifiers. The 2-μm CPA system displays an excellent stability with a pulse-to-pulse root mean square (rms) as low as 0.3%. The spectrum with a central wavelength of 2051 nm is well fitted by a Gaussian shape and shown in Fig. 2(a). Due to gain narrowing in the amplifier chain, the emission bandwidth is reduced to 2.5 nm (FWHM), supporting a ~2.8-ps FTL pulse duration. With a commercial auto correlator (APE), the chirped pulse duration was measured to 250 ps. The pulse energy for compression was limited to 26 mJ to prevent damage of the applied dielectrically coated gratings. The Treacy-type compressor de-chirps the amplified pulses with an efficiency of 77%, resulting in a compressed pulse energy of 20 mJ. The recorded autocorrelation trace

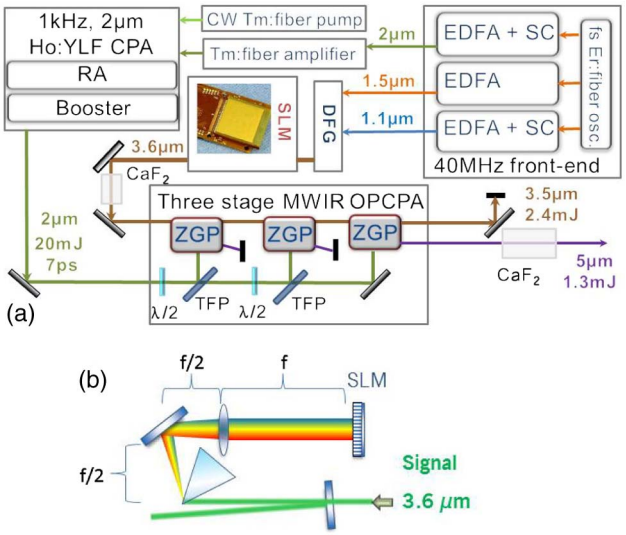

Fig. 1. (a) Setup of the MWIR OPCPA source pumped at 2 μm. The main parts are the Er:fiber-laser-based front end (EDFA), the difference frequency generation (DFG), the spatial light modulator (SLM), the 2-μm Ho:YLF CPA amplifiers, and the three OPA stages based on ZGP crystals. RA, regenerative amplifier; Booster, power amplifier; SC, supercontinuum generation; TFP, thin-film polarizer. (b) Design of the pulse shaper in a 4f configuration with the reflective SLM placed in its Fourier plane.

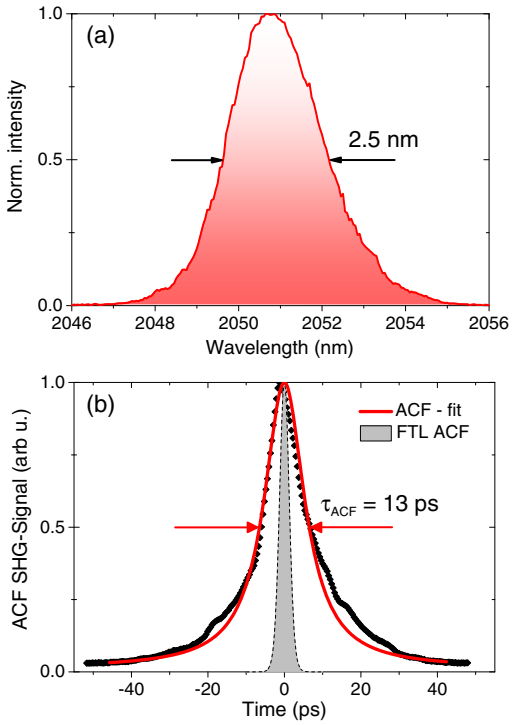

Fig. 2. Ho:YLF CPA amplifier performance at 1 kHz repetition rate. (a) Optical spectrum; (b) ACF of the compressed pulses at 20 mJ, measured and fit with a Lorentzian-shape profile.

(ACF) of the compressed pulse exhibits a FWHM of 13 ps and is shown in Fig. 2(b). The best fit is achieved using a Lorentzian-shape profile, which yields a pulse duration of 7 ps (FWHM). The beam quality after the booster amplifiers is measured to be better than a M^2 of 1.2 [12].

The signal pulse is generated via DFG with a duration of 27 fs and a spectrum extending from 2650 to 3950 nm at $1/e^2$ [Fig. 3(b)]. In the parametric amplifier chain, the 3.6-μm pulses are spectrally shaped by the SLM, stretched to 3 ps, and then delivered to the first OPA stage. The OPA chain is based on ZGP crystals and composed of three stages designed for different gain levels. The parameters of the three ZGP crystals can be found in Ref. [20]. The first and the second stage are built in non-collinear geometry. In the final stage, a collinear OPA design is chosen to prevent an angular dispersed idler. CaF_2 crystals are used as the stretcher and compressor for the signal pulse after the SLM and the idler pulses after amplification, respectively. The use of bulk materials resulted in an exceptionally low loss for the management of the main contribution of the second-order dispersion in the OPCPA. The emitted pulses by the OPCPA are characterized using the second-harmonic generation frequency-resolved optical gating (SHG-FROG) technique.

3. MWIR SLM

Spectral pulse shaping is performed using a MWIR SLM based on the liquid-crystal-on-silicon (LCOS) technology [23,24]. LCOS devices can be designed to manipulate optical pulses through phase-only modulation, e.g., they operate in reflection

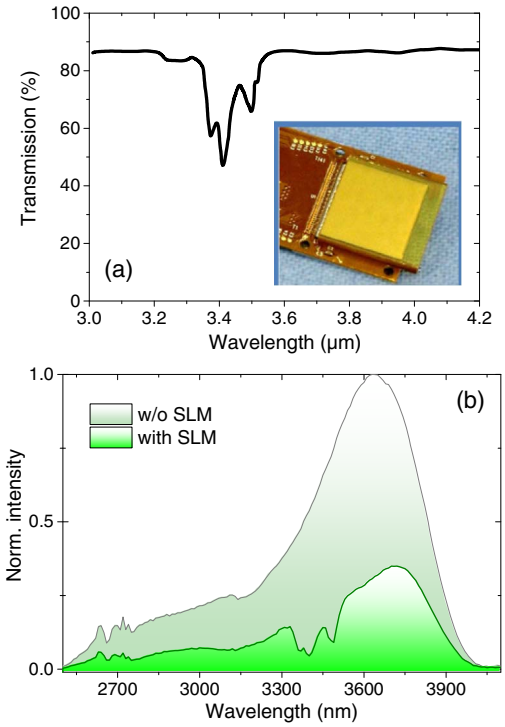

Fig. 3. (a) Transmission spectrum of the MWIR LCOS SLM in the range covered by the generated DFG. Inset: picture of the reflection-type LC array. (b) Spectrum of the signal pulse generated via DFG before and after passing the SLM.

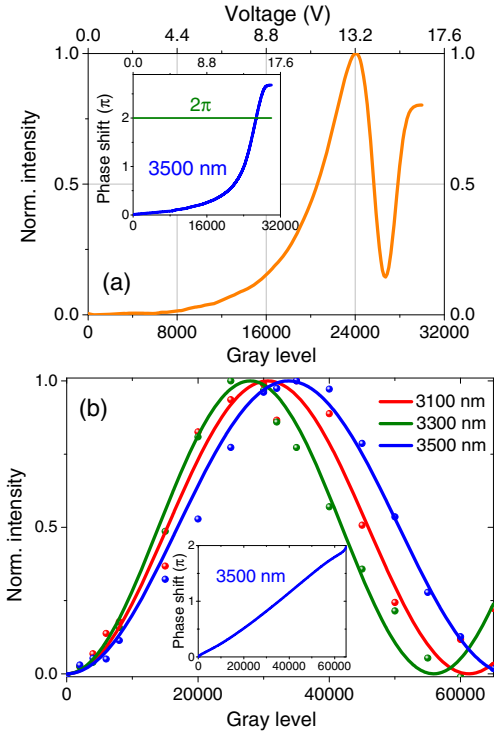

Fig. 4. Characterization of the MWIR SLM. (a) Measured intensity of the first diffraction order using a programmed binary grating in the LCOS device as a function of the applied voltage (gray level) at 3500 nm. Inset: extracted phase shift versus applied voltage (gray level) at 3500 nm. (b) Measured intensity of the first diffraction order using the calibrated and linearized phase response function via LUT at 3500 nm for three different wavelengths as a function of the applied voltage (gray level). Inset: extracted calibrated and linearized phase response curve at 3500 nm.

mode [25,26]. The LCOS-SLM (BNS) is designed for operating in the 2–7 μm wavelength range. The LC material is placed in a 14-μm thin cell between a ZnSe window and a silicon backplane. The LC array contains 512 × 512 pixels with a pitch of 37.5 μm. A picture of the reflection-type LCOS device is presented in Fig. 3(a) (inset). For our purpose, the SLM allows a more straightforward phase manipulation for the broadband signal pulses at 3.6 μm compared to the 5-μm idler pulses. The advantages of using our SLM at 3.6 μm compared to 5 μm are a lower absorption over the respective spectral range and a higher phase stroke. Due to the chirp transfer during parametric amplification, we indirectly manage the dispersion of the 5-μm idler pulses for recompression. The transmission spectrum of the LC array exhibits some absorption bands corresponding to the absorption characteristics of the embedded organic crystals. Note that these absorption bands are also present in nematic LC materials [24]. The LC transmission spectrum in the range covered by the generated DFG spectrum is shown in Fig. 3(a). The impact of the LC array absorption around 3.4 μm is clearly detectable in the signal pulse spectrum after passing the SLM [Fig. 3(b)].

The SLM is implemented in a typical $4f$ configuration using a sapphire prism as the dispersive element [Fig. 1(b)]. The pulse shaper design provides a throughput of 30%, much higher than the competing solution based on AOPDFs (<10%). The design of our pulse shaper setup resulted in a resolution of 10 nm for independent spectral shaping. The phase shift of the spectrally dispersed signal, achievable by passing the pulse shaper, depends on the transmitted wavelength and the applied voltage on the LC array. All these effects were analyzed and evaluated to calibrate the LC array. For calibration, a diffraction-based method is used, where the relationship between the optical diffraction efficiency of a binary-phase grating and the applied voltage (gray levels) are analyzed [26]. The phase-voltage calibration curves were generated for selected wavelengths in the range of the signal spectrum, i.e., from 3.1 to 3.8 μm. For each wavelength, the diffracted intensity in the first order is measured using an imaging spectrometer (Horiba Scientific) for a programmed binary grating in dependence on the applied voltage. The normalized intensity response in the first diffraction order for 3.5 μm is presented in Fig. 4(a). It should be noted that the valley point does not reach zero intensity, which is a direct consequence of the array structure of the LC, resulting in spatial phase non-uniformity [26]. The corresponding phase shift is extracted for each gray level using Eq. (1),

$$\eta_S = \sin^2\left(\frac{\pi \cdot \Delta n_{\mathrm{LC}} \cdot d_{\mathrm{LC}}}{\lambda}\right), \tag{1}$$

where η_s is the diffraction efficiency, d_{LC} the cell thickness, n_{LC} the refractive index of the LC, and λ the wavelength [25], and it is also shown in Fig. 4(a) (inset). The maximum phase correction stroke attainable at 3.5 μm is 2.7π. We limit the phase modulation within our 10 nm spectral resolution

(covering 10 pixels) to 2π and use a look-up table (LUT) to linearize the response curve. The latter is shown in Fig. 4(b) (inset) for the 3.5-μm calibration wavelength. After this procedure, a linear increase of the gray level between 0 and 65,536 corresponds to a linear phase shift between 0 and 2π at 3.5 μm. Applying the calibrated and linearized response curve, the diffracted intensity in the first order is recorded for three different wavelengths [Fig. 4(b)]. The sinusoidal shapes confirm the successful calibration procedure. Taking into account the spectral resolution of our shaper setup, the maximum phase shaping range for the signal spectrum amounts to ~100 rad. As indicated in Fig. 4(b), due to the refractive index change of the LC material in range of the signal spectrum, the phase stroke displays an additional wavelength dependence.

Beyond the described calibration procedure, the phase modulation of the SLM device can be influenced by additionally Gires–Tournois effects (GTI) due to the LCOS structure and/or non-perfect antireflection coating of the cover window [25]. Figure 5(a) displays the measured spectrally resolved phase response between 3.0 and 4.0 μm for a gray level of 32,768 (phase shift: π). A modulation of the spectral phase is recorded, indicating the GTI effect in the LCOS device, which is proved by a fit based on the GTI effect [Fig. 5(b)]. The latter occurs in addition to the linear increase of the maximum phase stroke towards shorter wavelengths, which is an inherent property of the device. The GTI effect has to be implemented in the SLM programming. Therefore, the following phase term describing the GTI effect is added [25]:

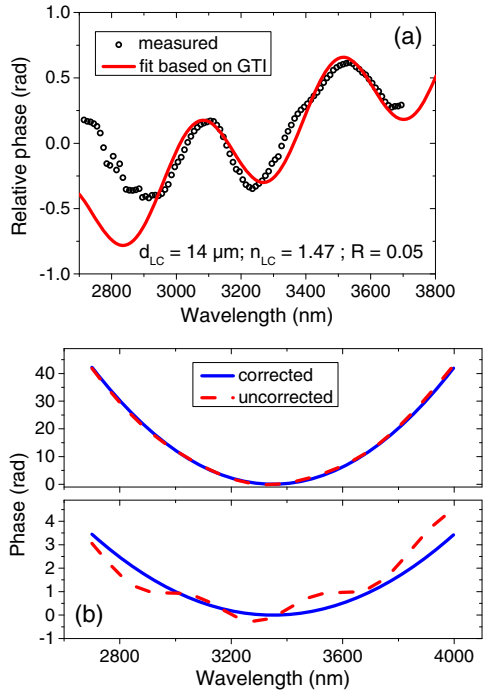

Fig. 5. Characterization of the MWIR spatial light modulator. (a) Measured spectrally resolved phase response between 3.0 and 4.0 μm for a gray level of 32,768 (phase shift: π). A fit based on the GTI effect is shown for comparison. (b) Simulation of the GTI effect's influence on the expected phase corrections in our OPCPA system; quadratic phase with and without GTI correction term for two phase correction scales.

$$\phi = 2 \arctan\left[-\frac{1+\sqrt{R}}{1-\sqrt{R}} \tan\left(\pi \frac{2d_{LC} \cdot n_{LC}(\lambda) \cdot \cos(\xi)}{\lambda}\right)\right], \quad (2)$$

with the reflectivity R of the front window, the cell thickness d_{LC}, the refractive index n_{LC} of the LCs, the internal incidence angle ξ, and the wavelength λ.

To illustrate the influence of the GTI effect on the expected phase corrections in our OPCPA system, Fig. 5(b) shows the simulated quadratic phase with and without the GTI correction term. If the total required phase shift is in the order of 2π, the GTI effect has to be taken into account. In our setup, the phase correction is in the order of 10π, so the influence the GTI effect is rather small.

4. MWIR OPCPA

In OPAs, the optimal pump to signal pulse duration is gain dependent [27]. Since the gain differs greatly in a multi-stage OPA, the signal pulse duration has to be adapted accordingly for each stage for optimal conversion efficiency and bandwidth. Seeded by the negatively chirped signal pulses and pumped by 0.3 mJ, the first stage provides 4.5-μJ signal pulses. To increase the conversion efficiency in the following OPA stages, the signal pulses are further stretched to 5 ps in front of the second stage. The second amplifier yields 250 μJ signal pulses for the chosen pump energy of 2.2 mJ. Applying 14 mJ of the available 2-μm pulse energy in the third stage, 2.4 and 1.3 mJ per pulse are generated in the signal at 3.5 μm and the idler at 5 μm, respectively. The idler spectrum displays a width of ~850 nm (FWHM) and supports a FTL pulse duration of 50 fs (without the SLM).

The SHG-FROG characterization of the compressed idler pulses in the case of pure bulk dispersion management in our OPCPA, e.g., without the SLM implemented, was performed earlier, and the results were published in Ref. [20]. The retrieved pulse shape with a duration of 160 fs exhibited a pronounced post-pulse structure indicating a relatively large amount of uncompensated third-order dispersion (TOD) but also higher orders. During parametric amplification, the generated idler exhibits an inverted sign of the group delay dispersion (GDD) relative to the signal, while the TOD does not reverse the sign. The remaining TOD cannot be compensated for by inserting further appropriate bulk material in the stretcher or compressor because of their always positive TOD.

To achieve shorter pulses in the few-cycle regime, the employment of active spectral phase control is obvious. After the implementation of the SLM in the setup (Fig. 1) we first tested its spectral phase tuning capabilities by phase-only shaping. The SLM has been programmed with different GDD and TOD values, and the resulting phase change of the idler pulse was measured by the SHG-FROG technique. An example of this examination is illustrated in Fig. 6 where the TOD is compensated for completely, whereas the GDD is changed from 0 to 5000 fs^2. Comparing Figs. 6(a) and 6(b), the measured phase change of the idler is consistent with that implemented by the SLM for the signal pulse. The deviation for wavelengths longer than ~5.5 μm is not related to the SLM and is discussed later.

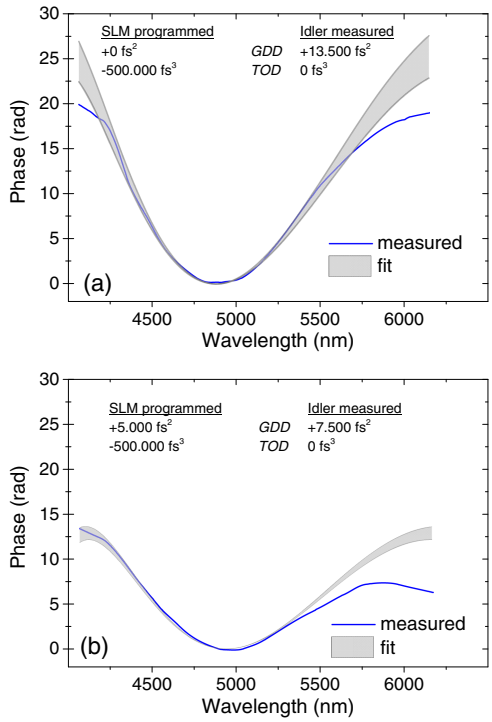

Fig. 6. Capabilities of indirect spectral shaping of the idler pulse by shaping the signal pulse by the MWIR SLM. The measured idler phase (SHG-FROG technique) is shown when the GDD is tuned from (a) +0 fs² to (b) +5000 fs² on the SLM. The gray area displays the best fit for the measured spectral phase.

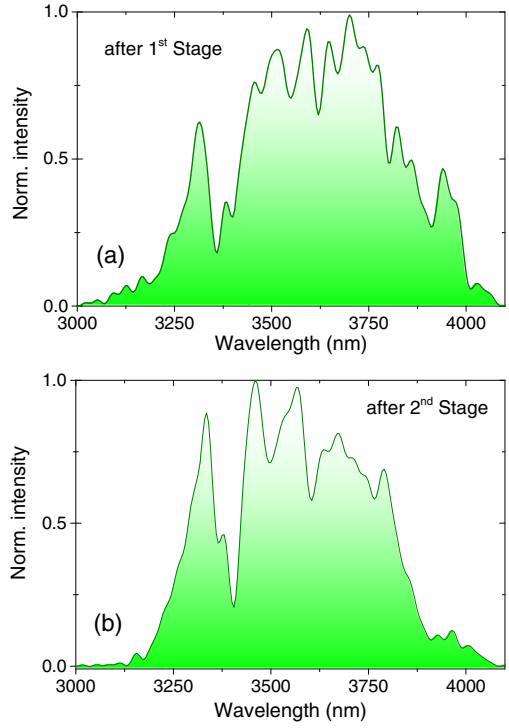

Fig. 7. Evolution of the signal spectrum after the (a) first and (b) second OPA stages.

After the careful calibration of the SLM, phase-only shaping of the signal pulses in the OPCPA is performed. Figure 7 shows the evolution of the signal spectrum after the first and second OPA stage. Compared to the seed spectrum [Fig. 3(b)], the bandwidth of the amplified signal spectrum is slightly reduced because of the limited OPA phase matching bandwidth in the first stage. No significant changes of the signal spectrum are detected upon amplification in the second and third stage. It is worth noting that the dip in the spectrum at 3.4 μm cannot be leveled out during the parametric amplification (Fig. 7).

The idler spectrum generated in the third stage, together with the theoretical idler spectrum calculated on the basis of the measured signal spectrum after the second stage, is presented in Fig. 8(a). The slightly reduced spectral intensity of the idler in the short wavelength part of the spectrum is related to the characteristics of the dichroic mirror used for separation of signal and idler. In addition to the dip in the spectrum related to the LC array absorption (in the idler spectrum at 5.2 μm), some structuring is observed. The strong bands can be clearly associated with distinct absorption characteristics of the atmosphere. In Fig. 8(b), the idler spectrum and the atmospheric absorption are shown. The band around 4.25 μm is related to CO_2 absorption, whereas the absorption lines above 5.5 μm originate from water vapor. The latter is not included in the simulated spectrum, which hence has a smooth shape [Fig. 8(a)]. Any additional structuring is attributed to diffraction on the LC array of the SLM. Nevertheless, the idler spectrum centered at 5.0 μm

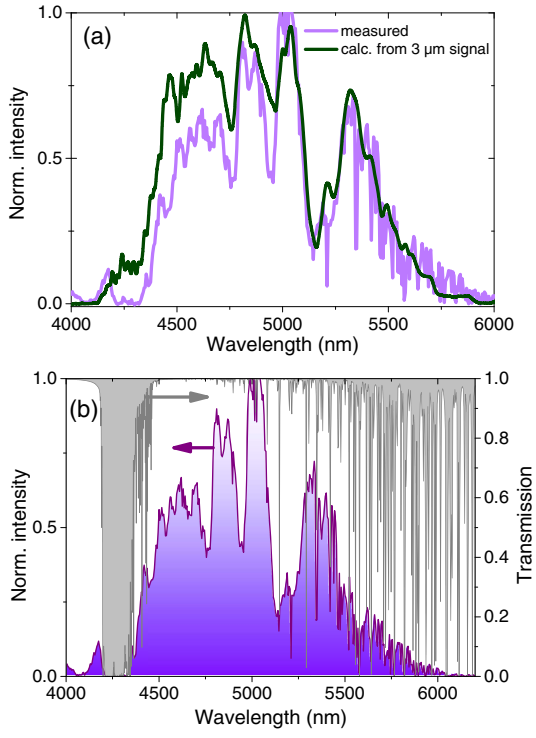

Fig. 8. (a) Measured idler spectrum after the third OPA stage, together with the calculated idler spectrum being based on the measured signal spectrum after the second OPA stage. (b) Measured idler spectrum (violet, arrow to the left) and the atmospheric absorption (gray, arrow to the right) in this range.

with a $1/e^2$ width of ~1300 nm still supports a FTL pulse duration of ~50 fs.

Compensating for the residual GDD, TOD, and fourth-order dispersion of the pulses by the SLM, successful recompression was achieved despite the different absorption components distorting the signal and idler spectra. The measured and retrieved SHG-FROG traces and the retrieval results are shown in Fig. 9. The measured SHG-FROG trace exhibits a slightly structured shape, which is related to the structures in the idler spectrum and the non-perfect beam pointing stability throughout the recording time (1 h). In the retrieved SHG-FROG trace this structuring is absent because of the resolution of the retrieval algorithm. The FROG error is <1%. The SHG-FROG trace indicates the absence of the red wing of the idler spectrum ascribed to the water vapor absorption in this range. The latter leads to large local phase modulations [28] and causes a reduced SHG-intensity level, which lies below the dynamic range of the SHG measurement setup. As a consequence, the red wing of the spectrum does not contribute to the compressed pulse, as confirmed by the retrieved optical spectrum [Fig. 9(c)]. Nevertheless, the flat spectral phase verifies the excellent pulse quality [Fig. 9(c)]. The retrieved pulse shape yields a pulse duration of 80 ± 2 fs (FWHM) with an estimated energy content of 77% [Fig. 9(d)]. The recompressed pulses are not perfectly clean, but contain a small pedestal corresponding to the above described modulations in the spectrum. The estimated energy in the main peak amounts to a sizeable value of 1.0 mJ. The derived peak power of 10 GW represents the highest achieved for OPCPAs beyond 4 μm so far. The beam profile is nearly diffraction limited.

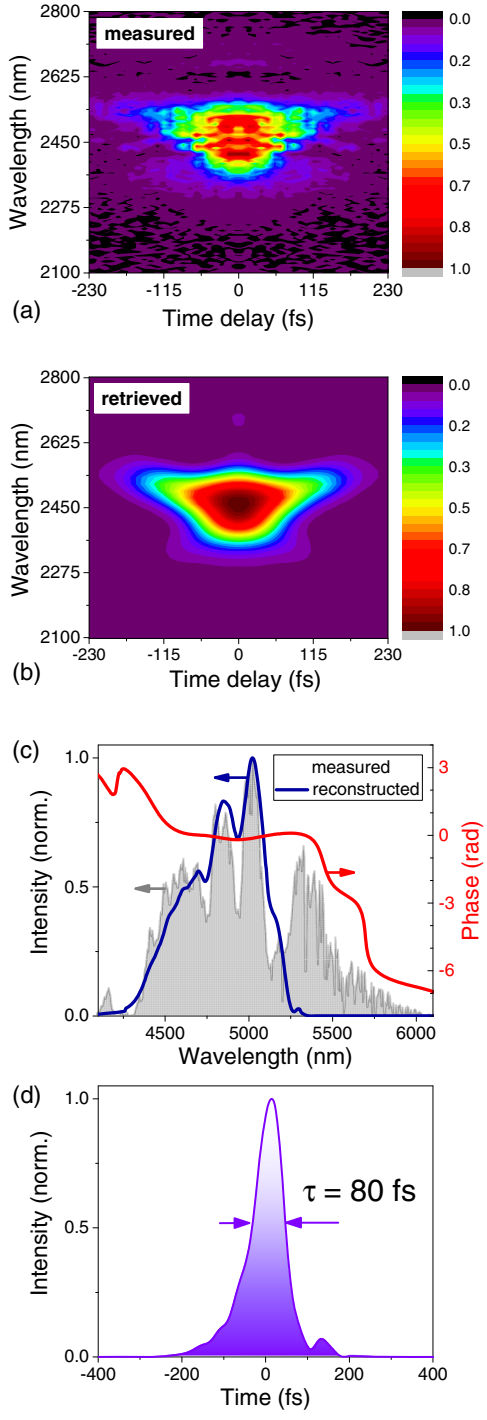

Fig. 9. SHG-FROG characterization of the compressed 5-μm pulses at a 1-mJ energy level. (a), (b) SHG-FROG trace measured and retrieved. (c) Optical spectrum, measured (gray), retrieved (blue), and phase (red). (d) Retrieved temporal pulse shape.

5. CONCLUSION

In conclusion, we have demonstrated the capabilities of spectral pulse shaping in the MWIR using a LCOS-based SLM for the generation of few-cycle pulses. After careful calibration of the LC array response in the wavelength range between 3.0 and 4.0 μm, the SLM is used as a phase-only shaper for the >1000-nm broad spectrum ($1/e^2$ level) of the signal pulses in our MWIR OPCPA. In combination with pure bulk dispersion management in the OPCPA, the active phase manipulation allows for a flexible adaptation to the residual spectral phase for the idler centered at 5 μm thanks to the chirp transfer in parametric amplifiers. This adaptive pulse compression mechanism leads to idler pulse durations as short as 80 fs corresponding to less than five optical cycles. The generated pulse energy of sizeable 1.0 mJ translates into a peak power of 10 GW, representing the highest for 5-μm OPCPA systems. The system appears scalable with respect to higher pulse peak power by purging the parametric amplifier chain (e.g., with nitrogen) to get access to the full generated optical spectrum and thus to a potential shorter duration of the compressed pulses.

Funding. Leibniz-Gemeinschaft (SAW-2014-MBI-1); Horizon 2020 Framework Programme (H2020) (654148).

Acknowledgment. We acknowledge the expert technical support by Dennis Ueberschär, Max Born Institute, Berlin, Germany.

REFERENCES

1. B. Wolter, M. G. Pullen, M. Baudisch, M. Sclafani, M. Hemmer, A. Senftleben, C. D. Schröter, J. Ullrich, R. Moshammer, and J. Biegert, "Strong-field physics with mid-IR fields," Phys. Rev. X **5**, 021034 (2015).

2. T. Popmintchev, M.-C. Chen, D. Popmintchev, P. Arpin, S. Brown, S. Ališauskas, G. Andriukaitis, T. Balčiunas, O. D. Mücke, A. Pugzlys, A. Baltuška, B. Shim, S. E. Schrauth, A. Gaeta, C. Hernández-García, L. Plaja, A. Becker, A. Jaron-Becker, M. M. Murnane, and H. C. Kapteyn, "Bright coherent ultrahigh harmonics in the keV X-ray regime from mid-infrared femtosecond lasers," Science **336**, 1287–1291 (2012).
3. C. Calabrese, A. M. Stingel, L. Shen, and P. B. Petersen, "Ultrafast continuum mid-infrared spectroscopy: probing the entire vibrational spectrum in a single laser shot with femtosecond time resolution," Opt. Lett. **37**, 2265–2267 (2012).
4. K.-H. Hong, C.-J. Lai, J. P. Siqueira, P. Krogen, J. Moses, C.-L. Chang, G. J. Stein, L. E. Zapata, and F. X. Kärtner, "Multi-mJ, kHz, 2.1 μm optical parametric chirped-pulse amplifier and high-flux soft x-ray high-harmonic generation," Opt. Lett. **39**, 3145–3148 (2014).
5. J. Weisshaupt, V. Juvé, M. Holtz, S. A. Ku, M. Woerner, T. Elsaesser, S. Ališauskas, A. Pugžlys, and A. Baltuška, "High-brightness table-top hard x-ray source driven by sub-100 femtosecond mid-infrared pulses," Nat. Photonics **8**, 927–930 (2014).
6. V. Petrov, "Frequency down-conversion of solid-state laser sources to the mid-infrared spectral range using non-oxide nonlinear crystals," Prog. Quantum Electron. **42**, 1–106 (2015).
7. G. Andriukaitis, T. Balčiunas, S. Ališauskas, A. Pugžlys, A. Baltuška, T. Popmintchev, M.-C. Chen, M. M. Murnane, and H. C. Kapteyn, "90 GW peak power few-cycle mid-infrared pulses from an optical parametric amplifier," Opt. Lett. **36**, 2755–2757 (2011).
8. M. Baudisch, H. Pires, H. Ishizuki, T. Taira, M. Hemmer, and J. Biegert, "Sub-4-optical-cycle, 340 MW peak power, high stability mid-IR source at 160 kHz," J. Opt. **17**, 094002 (2015).
9. M. Mero and V. Petrov, "High-power, few-cycle angular dispersion compensated mid-infrared pulses from a noncollinear optical parametric amplifier," IEEE Photon. J. **93**, 200408 (2017).
10. P. Wang, Y. Li, W. Li, H. Su, B. Shao, S. Li, C. Wang, D. Wang, R. Zhao, Y. Peng, Y. Leng, R. Li, and Z. Xu, "2.6 mJ/100 Hz CEP-stable near-single-cycle 4 μm laser based on OPCPA and hollow-core fiber compression," Opt. Lett. **43**, 2197–2200 (2018).
11. P. G. Schunemann, K. T. Zawilski, L. A. Pomeranz, D. J. Creeden, and P. A. Budni, "Advances in nonlinear optical crystals for mid-infrared coherent sources," J. Opt. Soc. Am. B **33**, D36–D43 (2016).
12. L. von Grafenstein, M. Bock, D. Ueberschaer, U. Griebner, and T. Elsaesser, "Ho:YLF chirped pulse amplification at kilohertz repetition rates—4.3 ps pulses at 2 μm with GW peak power," Opt. Lett. **41**, 4668–4671 (2016).
13. S. Demmler, J. Rothhardt, A. M. Heidt, A. Hartung, E. G. Rohwer, H. Bartelt, J. Limpert, and A. Tuennermann, "Generation of high quality, 1.3 cycle pulses by active phase control of an octave spanning supercontinuum," Opt. Express **19**, 20151–20158 (2011).
14. B. Xu, Y. Coello, V. V. Lozovoy, D. A. Harris, and M. Dantus, "Pulse shaping of octave spanning femtosecond laser pulses," Opt. Express **14**, 10939–10944 (2006).
15. K. Yamane, Z. Zhang, K. Oka, R. Morita, M. Yamashita, and A. Suguro, "Optical pulse compression to 3.4 fs in the monocycle region by feedback phase compensation," Opt. Lett. **28**, 2258–2260 (2003).
16. B. Schenkel, J. Biegert, U. Keller, C. Vozzi, M. Nisoli, G. Sansone, S. Stagira, S. De Silvestri, and O. Svelto, "Generation of 3.8-fs pulses from adaptive compression of a cascaded hollow fiber supercontinuum," Opt. Lett. **28**, 1987–1989 (2003).
17. A. Prakelt, M. Wollenhaupt, A. Assion, C. Horn, C. Sarpe-Tudoran, M. Winter, and T. Baumert, "Compact, robust, and flexible setup for femtosecond pulse shaping," Rev. Sci. Instrum. **74**, 4950–4953 (2003).
18. H. Liang, P. Krogen, Z. Wang, H. Park, T. Kroh, K. Zawilski, P. Schunemann, J. Moses, L. F. DiMauro, F. X. Kärtner, and K.-H. Hong, "High-energy mid-infrared sub-cycle pulse synthesis from a parametric amplifier," Nat. Commun. **8**, 141 (2017).
19. T. Kanai, P. Malevich, S. S. Kangaparambil, K. Ishida, M. Mizui, K. Yamanouchi, H. Hoogland, R. Holzwarth, A. Pugžlys, and A. Baltuška, "Parametric amplification of 100 fs mid-infrared pulses in $ZnGeP_2$ driven by a Ho:YAG chirped pulse amplifier," Opt. Lett. **42**, 683–686 (2017).
20. L. von Grafenstein, M. Bock, D. Ueberschaer, K. Zawilski, P. Schunemann, U. Griebner, and T. Elsaesser, "5 μm, few-cycle pulses with multi-GW peak power at a 1 kHz repetition rate," Opt. Lett. **42**, 3796–3799 (2017).
21. D. Sanchez, M. Hemmer, M. Baudisch, S. L. Cousin, K. Zawilski, P. Schunemann, O. Chalus, C. Simon-Boisson, and J. Biegert, "7 μm, ultrafast, sub-millijoule-level mid-infrared optical parametric chirped pulse amplifier pumped at 2 μm," Optica **3**, 147–150 (2016).
22. S. Wandel, M.-W. Lin, Y. Yin, G. Xu, and I. Jovanovic, "Parametric generation and characterization of femtosecond mid-infrared pulses in $ZnGeP_2$," Opt. Express **24**, 5287–5299 (2016).
23. S. Serati, T. K. Ewing, and J. Stockley, "New developments in high-resolution liquid-crystal spatial light modulators for wavefront control," Proc. SPIE **4825**, 46–55 (2002).
24. T. K. Ewing and W. R. Folks, "Liquid crystal on silicon infrared scene projectors," Proc. SPIE **5785**, 36–45 (2005).
25. M. Bock, S. K. Das, R. Grunwald, S. Osten, P. Staudt, and G. Stibenz, "Spectral and temporal response of liquid-crystal-on-silicon spatial light modulators," Appl. Phys. Lett. **92**, 151105 (2008).
26. Z. Zhang, H. Yang, B. Robertson, M. Redmond, M. Pivnenko, N. Collings, W. A. Crossland, and D. Chu, "Diffraction based phase compensation method for phase-only liquid crystal on silicon devices in operation," Appl. Opt. **51**, 3837–3846 (2012).
27. G. Cerullo and S. De Silvestri, "Ultrafast optical parametric amplifiers," Rev. Sci. Instrum. **74**, 1–18 (2003).
28. M. Gebhardt, C. Gaida, F. Stutzki, S. Hädrich, C. Jauregui, J. Limpert, and A. Tünnermann, "Impact of atmospheric molecular absorption on the temporal and spatial evolution of ultra-short optical pulses," Opt. Express **23**, 13776–13787 (2015).